524 *Chem. Mater.* **2010,** *22,* 524–531
DOI:10.1021/cm9031623

CHEMISTRY OF MATERIALS
Article

A Molybdenum Dithiolene Complex as *p*-Dopant for Hole-Transport Materials: A Multitechnique Experimental and Theoretical Investigation

Yabing Qi,*[,†] Tissa Sajoto,[‡] Michael Kröger,[†,§] Alexander M. Kandabarow,[†,△] Wonjun Park,[†,#] Stephen Barlow,[‡] Eung-Gun Kim,[‡] Leszek Wielunski,[∥,⊥] L. C. Feldman,[∥,⊥] Robert A. Bartynski,[∥,⊥] Jean-Luc Brédas,[‡] Seth R. Marder,[‡] and Antoine Kahn[†]

[†]*Department of Electrical Engineering, Princeton University, Princeton, New Jersey 08544,* [‡]*School of Chemistry and Biochemistry and Center for Organic Electronics and Photonics, Georgia Institute of Technology, Atlanta, Georgia 30332,* [∥]*Department of Physics and Astronomy, Rutgers University, Piscataway, New Jersey 08854, and* [⊥]*Institute for Advanced Materials Devices and Nanotechnology, Rutgers University, Piscataway, New Jersey 08854.* [§]*Now at Innovation Lab GmbH, Heidelberg, Germany.* [△]*Now at ZS Associates, Chicago, IL.* [#]*Now at School of Electrical and Computer Engineering in Purdue University.*

Received October 14, 2009. Revised Manuscript Received November 16, 2009

Molybdenum tris-[1,2-bis(trifluoromethyl)ethane-1,2-dithiolene] ($Mo(tfd)_3$) is investigated as a *p*-dopant for organic semiconductors. With an electron affinity of 5.6 eV, $Mo(tfd)_3$ is a strong oxidizing agent suitable for the oxidation of several hole transport materials (HTMs). Ultraviolet photoemission spectroscopy confirms *p*-doping of the standard HTM *N*,*N*′-di-[(1-naphthyl)-*N*,*N*′-diphenyl]-1,1′-biphenyl-4,4′-diamine (α-NPD). Strong enhancement of hole injection at α-NPD/Au interfaces is achieved via doping-induced formation of a narrow depletion region in the organic semiconductor. Variable-temperature current−voltage measurements on α-NPD: $Mo(tfd)_3$ (0−3.8 mol %) yield an activation energy for polaron transport that decreases with increasing doping concentration, which is consistent with the effect of the doping-induced filling of traps on hopping transport. Good stability of $Mo(tfd)_3$ versus diffusion in the α-NPD host matrix is demonstrated by Rutherford backscattering for temperatures up to 110 °C. Density functional theory (DFT) calculations are performed to obtain geometries and electronic structures of isolated neutral and anionic $Mo(tfd)_3$ molecules.

1. Introduction

Electrical doping of organic films holds great promise for enhancing carrier injection and improving bulk charge transport in a variety of molecular- and polymer-based materials.[1−6] With the recent technological innovations in organic devices, the search for efficient and stable dopants that are best-suited for these semiconductors is attracting considerable interest.[3,4,7,8] Several inorganic and organic dopants have been developed over the past decade, and doping has been demonstrated in a variety of molecular and polymer semiconductors via spectroscopic and charge carrier transport methods.[3,5,8−14] The efficiency of dopants and their stability, with respect to diffusion, are complex functions of their electronic structure on one hand, and functions of size and shape on the other hand. F_4-TCNQ (which denotes 2,3,5,6-tetrafluoro-7,7,8,8-tetracyanoquinodimethane) is a well-known *p*-type dopant with an electron affinity (EA) of 5.24 eV, [2,3,12,13] which is sufficient to dope several commonly used hole transport materials (HTMs), such as metal phthalocyanines and *N*,*N*′-di-[(1-naphthyl)-*N*,*N*′-diphenyl]-1,1′-biphenyl-4,4′-diamine (α-NPD; see Figure 1a). Yet, instability with regard to diffusion has somewhat hindered its use in organic electronics.[15−17]

In this paper, we present a detailed experimental study of the performance of molybdenum tris-[1,2-bis(trifluoromethyl)ethane-1,2-dithiolene] ($Mo(tfd)_3$; see Figure 1a),[18]

*Author to whom correspondence should be addressed. E-mail address: yqi@princeton.edu.

(1) Lous, E.; Blom, P.; Molenkamp, L.; de Leeuw, D. *Phys. Rev. B* **1995**, *51*, 17251–17254.
(2) Gao, W. Y.; Kahn, A. *J. Appl. Phys.* **2003**, *94*, 359–366.
(3) Abe, Y.; Hasegawa, T.; Takahashi, Y.; Yamada, T.; Tokura, Y. *Appl. Phys. Lett.* **2005**, *87*, 153506.
(4) Chan, C. K.; Kahn, A.; Zhang, Q.; Barlow, S.; Marder, S. R. *J. Appl. Phys.* **2007**, *102*, 014906.
(5) Porter, W. W.; Vaid, T. P. *J. Mater. Chem.* **2007**, *17*, 469–475.
(6) Kröger, M.; Hamwi, S.; Meyer, J.; Riedl, T.; Kowalsky, W.; Kahn, A. *Org. Electron.* **2009**, *10*, 932–938.
(7) Walzer, K.; Maennig, B.; Pfeiffer, M.; Leo, K. *Chem. Rev.* **2007**, *107*, 1233–1271.
(8) Gao, W. Y.; Kahn, A. *J. Phys. Condens. Matter* **2003**, *15*, S2757–S2770.
(9) Anthopoulos, T. D.; Shafai, T. S. *Appl. Phys. Lett.* **2003**, *82*, 1628–1630.
(10) Lu, C.-K.; Meng, H.-F. *Phys. Rev. B* **2007**, *75*, 235206.
(11) Xie, G.; Meng, Y.; Wu, F.; Tao, C.; Zhang, D.; Liu, M.; Xue, Q.; Chen, W.; Zhao, Y. *Appl. Phys. Lett.* **2008**, *92*, 093305.
(12) Vanoni, C.; Tsujino, S.; Jung, T. A. *Appl. Phys. Lett.* **2007**, *90*, 193119.
(13) Yim, K.-H.; Murphy, C. E.; Halls, J.; Burroughes, J. H.; Friend, R.; Kim, J.-S. *Adv. Mater.* **2008**, *20*, 3319–3324.
(14) Kröger, M.; Hamwi, S.; Meyer, J.; Riedl, T.; Kowalsky, W.; Kahn, A. *Appl. Phys. Lett.* **2009**, *95*, 123301.
(15) Drechsel, J.; Pfeiffer, M.; Zhou, X.; Nollau, A.; Leo, K. *Synth. Met.* **2002**, *127*, 201–205.
(16) Wellmann, P.; Hofmann, M.; Zeika, O.; Werner, A.; Birnstock, J.; Meerheim, R.; He, G.; Walzer, K.; Pfeiffer, M.; Leo, K. *Inf. Disp.* **2005**, *13*, 393.
(17) Gao, Z. Q.; Mi, B. X.; Xu, G. Z.; Wan, Y. Q.; Gong, M. L.; Cheah, K. W.; Chen, C. H. *Chem. Commun.* **2008**, 117–119.
(18) King, R. B. *Inorg. Chem.* **1963**, *2*, 641.

 Published on Web 12/16/2009 © 2009 American Chemical Society

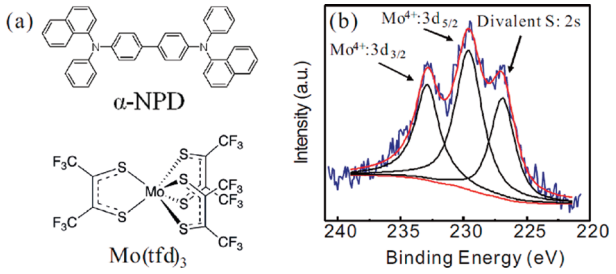

Figure 1. (a) Chemical structures of α-NPD and $Mo(tfd)_3$. (b) XPS 3d spectral region of Mo measured on a pure $Mo(tfd)_3$ film (~9 nm) on Au.

as a *p*-type dopant. This compound has previously been recognized as a useful solution oxidant,[19] and solution electrochemical data suggest that this species is a more powerful oxidant than F_4-TCNQ.[20] Moreover, our previous investigations of this electron-accepting molecule, using ultraviolet photoemission spectroscopy (UPS) and inverse photoemission spectroscopy (IPES), coupled with density functional theory (DFT), have provided insight into its potential as a *p*-dopant for HTMs, in particular, its ionization energy (IE) and electron affinity (EA).[20] The electron affinity (EA) of $Mo(tfd)_3$ in condensed form was determined to be 5.6 eV (i.e., 0.35 eV greater than that of F_4-TCNQ), and room-temperature current−voltage ($I-V$) measurements have shown effective *p*-doping of α-NPD (IE = 5.4 eV),[21] while the enhancement of conductivity in another amine hole-transport material has been reported in a patent.[22] Here, we further investigate the use of $Mo(tfd)_3$ to dope organic semiconductors at the interfaces with electrodes, to enhance charge carrier injection. X-ray photoelectron spectroscopy (XPS) provides information on the effective oxidation state of Mo in the molecule. Variable-temperature $I-V$ (VTIV) measurements are performed on α-NPD:$Mo(tfd)_3$ films to explore charge-transport mechanisms. The Fermi level position shift versus doping concentration is confirmed via UPS. In addition, the large atomic mass of Mo is advantageously used to probe the position of $Mo(tfd)_3$ molecules via Rutherford backscattering (RBS), as a function of annealing of the doped film. The $Mo(tfd)_3$ molecule is determined to be stable, with respect to diffusion, even at elevated temperature; this is a result of its bulkier and nonplanar structure, which bodes well for its application as an effective dopant. The diffusional stability of dopant in the host matrix is further supported by the size increase of the $Mo(tfd)_3$ molecule calculated by DFT upon the formation of its anion.

(19) Connelly, N.; Geiger, W. *Chem. Rev.* **1996**, *96*, 877–910.
(20) Qi, Y.; Sajoto, T.; Barlow, S.; Kim, E.-G.; Brédas, J.-L.; Marder, S. R.; Kahn, A. *J. Am. Chem. Soc.* **2009**, *131*, 12530–12531.
(21) It is worth noting that IP and EA data suggest an exergonic electron-transfer from α-NPD to $Mo(tfd)_3$ in the solid state (ΔG = ca. −20 kJ/mol), whereas electrochemical data suggest a slightly endogonic reaction in dichloromethane (ca. +4 kJ/mol), thus emphasizing the importance of solid-state IP and EA measurements in assessing dopant strength.
(22) Zeika, O.; Werner, A.; Hartmann, H.; Willmann, S. PCT Application WO 061517, **2008**.

2. Experimental and Theoretical Methods

$Mo(tfd)_3$ was prepared from molybdenum hexacarbonyl and bis(trifluoro)dithieteneby[23] in methylcyclohexane, according to literature procedures,[24] and purified by Soxhlet extraction into pentane.[24] UPS, XPS, and in situ room-temperature $I-V$ measurements were performed in a three-chamber ultrahigh-vacuum (UHV) system composed of a growth chamber that was equipped with organic evaporation stations (base pressure of $\sim 10^{-9}$ Torr), a central chamber for sample introduction, deposition of doped films, and in situ $I-V$ measurements (base pressure of $\sim 5 \times 10^{-10}$ Torr), and an analysis chamber (base pressure = 10^{-10} Torr) for UPS and XPS measurements. Substrates for these measurements were prepared by evaporating a 5-nm Ti adhesion layer on Si, followed by ~200 nm of Au. They were cleaned in boiling acetone and methanol, and then transferred into the vacuum system. Pure $Mo(tfd)_3$ films (6−9 nm) were deposited on Au for studies of the electronic structure and oxidation state. α-NPD films (5−10 nm) doped with various amounts of $Mo(tfd)_3$ were grown at room temperature via controlled coevaporation of the two molecular species for UPS measurements. Thick undoped and doped films (~170 nm), capped with Au top contacts, were grown for in situ $I-V$ measurements.

UPS was performed using both He(I) and He(II) photon lines (21.22 and 40.81 eV, respectively) from a He discharge lamp. The photon flux was kept low, to prevent damage to the organic films. XPS measurements were performed using the Al Kα line (1486.6 eV). Energy resolutions in UPS and XPS were 0.15 and 0.8 eV, respectively.[25]

VTIV measurements were performed in a two-chamber UHV system comprising a growth chamber for evaporating undoped and doped films (at a base pressure of 10^{-9} Torr) and an analysis chamber (at a base pressure of 5×10^{-10} Torr) equipped with a temperature-controlled sample stage (60 K < T < 340 K) for $I-V$ measurements. Films (200−500 nm thick) of undoped and doped α-NPD (dopant concentration $[Mo(tfd)_3] = 0-3.8$ mol %) were evaporated in the growth chamber on a pattern of gold electrodes (150-μm gaps between electrodes) predeposited on quartz. The samples were then transferred without breaking the vacuum to the temperature-controlled stage for VTIV measurements.

RBS measurements were performed at Rutgers University on two types of samples prepared at Princeton University and transported under dry nitrogen: (i) α-NPD (1000 Å)/α-NPD:2 mol % $Mo(tfd)_3$ (550 Å)/Si(100) and (ii) α-NPD (1500 Å)/α-NPD:2 mol % $Mo(tfd)_3$ (400 Å)/α-NPD (1500 Å)/Si(100). The latter were annealed for 15 min in dry nitrogen at 70, 90, or 110 °C. RBS analysis was performed with 2 MeV He ions from the Rutgers 1.7 MV Tandem accelerator. The ion beam was directed normal to the sample surface and two silicon surface barrier detectors were used in typical backscattering geometry (BA) and at the glancing exit angle (GAD) to improve measurement depth resolution. The scattering angles were 152° for BA and 105° for GAD. The depth resolution for Mo detection in NPD organic was ~38 nm for BA detector spectra and ~16 nm for GAD data. The RBS data analysis was performed using the SIMNRA computer program.[26]

(23) Krespan, N. G.; Geiger, W. E. *J. Am. Chem. Soc.* **1961**, *83*, 3434.
(24) Davison, A.; Holm, R. H.; Benson, R. E.; Mahler, M. *Inorg. Synth.* **1967**, *10*, 8.
(25) Wu, C. I.; Hirose, Y.; Sirringhaus, H.; Kahn, A. *Chem. Phys. Lett.* **1997**, *272*, 43–47.
(26) Mayer, M. AIP Conf. Proc. **1999**, *475*, 541.

The geometries and electronic structures of isolated neutral and anionic $Mo(tfd)_3$ molecules were optimized using DFT methods at the B3LYP level. The LANL2DZ basis set with the effective core potential was used for Mo and 6-31G(d) for S, C, and F. For the anion, a single-point, restricted open-shell calculation was also performed at the unrestricted open shell geometry. Atomic charges and electronic configurations were calculated using natural population analysis. The molecular volume was estimated by calculating the volume inside a contour of 0.001 electrons/Bohr^3. All DFT calculations were performed using the Gaussian 03 package.[27]

3. Results and Discussion

The 3d spectral region of Mo was examined by XPS on a pure $Mo(tfd)_3$ film (with a thickness of ~9 nm) evaporated on Au (see Figure 1b). The two peaks at binding energies of 229.6 and 232.9 eV correspond to the spin−orbit split $3d_{5/2}$ and $3d_{3/2}$ levels of Mo, respectively. The additional peak at 226.9 eV is attributable to the 2s level of S in $Mo(tfd)_3$ molecules. The black curves in Figure 1b represent fittings to the experimental data, with a statistical branching ratio of 3:2 for the peak areas of the $3d_{5/2}$ and $3d_{3/2}$ levels. The Mo binding energies can be compared with those of a wide range of model compounds of varying oxidation states[28] and fall within the range found for Mo(III) and Mo(IV) compounds, intermediate between the extreme values of 6+ and 0 that are suggested by metal tris(dithiolate) and metal tris(dithione) limiting structures, respectively. Moreover, the binding energies of both Mo and S peaks are very similar to those measured for MoS_2 by Turner et al.[29] (see Table 1), which is consistent with an effective Mo oxidation state of 4+. Previous studies of metal tris(dithiolene)s, in which significantly mixed metal d and ligand character for several of the frontier filled orbitals preclude facile assignment of oxidation state, suggest structures intermediate between the metal(VI) and metal(0) extremes.[30] In particular, experimental and theoretical data for other molybdenum tris(thiolene)s have been used to infer oxidation states of 4+ or 5+.[31−33]

Table 1. Binding Energies of Mo and S Levels

	Energy (eV)	
level	this work	MoS_2[a]
S (2s)	226.9	227.04
Mo ($3d_{5/2}$)	229.6	229.76
Mo ($3d_{5/2}$)	232.9	232.82

[a] Data taken from ref 29.

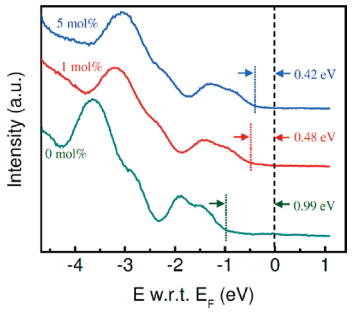

Figure 2. He I UPS spectra of α-NPD doped with 0, 1, and 5 mol % of $Mo(tfd)_3$, respectively.

The EA value of 5.6 eV for $Mo(tfd)_3$[20] is sufficiently large to *p*-dope several HTMs. This is demonstrated here by the shift of the α-NPD valence molecular levels toward the Fermi level with increasing doping concentration (see Figure 2). The energy difference between the Fermi level and the highest occupied molecular orbital (HOMO) edge ($E_F - E_{HOMO}$) decreases from 0.99 eV for the undoped film to a saturation value of 0.42 eV at 5 mol %. The shape of the filled-state spectrum remains essentially unperturbed by doping, except for a slight broadening of the molecular features. No additional states are observed for these dopant concentrations in the gap of the semiconductor. While the value of $E_F - E_{HOMO} = 0.99$ eV that was found for the undoped film results solely from the α-NPD/Au interface energetics, one might have expected the Fermi level to approach the HOMO edge more closely at high doping concentrations. However, the saturation value of 0.42 eV is very similar to the ~0.40 eV value noticed for F_4-TCNQ-doped α-NPD, even though $Mo(tfd)_3$, unlike F_4-TCNQ, has an EA value that is *larger* than the IE value of α-NPD. The saturation effect is equivalent to pinning of the Fermi level within a certain energy from the filled states. Fermi level pinning has been observed in the context of interface formation between organic semiconductors and electrodes with varying work functions, for both small molecules and polymers.[34−36] We attribute this effect to the tail of states, because of static and/or dynamic disorder in the molecular films,

(27) Frisch, M. J.; Trucks, G. W.; Schlegel, H. B.; Scuseria, G. E.; Robb, M. A.; Cheeseman, J. R.; Montgomery, J. A., Jr.; Vreven, T.; Kudin, K. N.; Burant, J. C.; Millam, J. M.; Iyengar, S. S.; Tomasi, J.; Barone, V.; Mennucci, B.; Cossi, M.; Scalmani, G.; Rega, N.; Petersson, G. A.; Nakatsuji, H.; Hada, M.; Ehara, M.; Toyota, K.; Fukuda, R.; Hasegawa, J.; Ishida, M.; Nakajima, T.; Honda, Y.; Kitao, O.; Nakai, H.; Klene, M.; Li, X.; Knox, J. E.; Hratchian, H. P.; Cross, J. B.; Bakken, V.; Adamo, C.; Jaramillo, J.; Gomperts, R.; Stratmann, R. E.; Yazyev, O.; Austin, A. J.; Cammi, R.; Pomelli, C.; Ochterski, J. W.; Ayala, P. Y.; Morokuma, K.; Voth, G. A.; Salvador, P.; Dannenberg, J. J.; Zakrzewski, V. G.; Dapprich, S.; Daniels, A. D.; Strain, M. C.; Farkas, O.; Malick, D. K.; Rabuck, A. D.; Raghavachari, K.; Foresman, J. B.; Ortiz, J. V.; Cui, Q.; Baboul, A. G.; Clifford, S.; Cioslowski, J.; Stefanov, B. B.; Liu, G.; Liashenko, A.; Piskorz, P.; Komaromi, I.; Martin, R. L.; Fox, D. J.; Keith, T.; Al-Laham, M. A.; Peng, C. Y.; Nanayakkara, A.; Challacombe, M.; Gill, P. M. W.; Johnson, B.; Chen, W.; Wong, M. W.; Gonzalez, C.; Pople, J. A. Gaussian 03, Revision C.02; Gaussian, Inc.: Wallingford, CT, **2004**.
(28) Burgmayer, S.; Kaufmann, H.; Fortunato, G.; Hug, P.; Fischer, B. *Inorg. Chem.* **1999**, *38*, 2607–2613.
(29) Turner, N. H.; Single, A. M. *Surf. Interface Anal.* **1990**, *15*, 215.
(30) Stiefel, E. I.; Eisenberg, R.; Rosenberg, R. C.; Gray, H. B. *J. Am. Chem. Soc.* **1966**, *88*, 2956.
(31) Davison, A.; Edelstein, N.; Holm, R. H.; Maki, A. H. *J. Am. Chem. Soc.* **1964**, *86*, 2799.
(32) Tenderholt, A.; Szilagyi, R.; Holm, R.; Hodgson, K.; Hedman, B.; Solomon, E. *Inorg. Chem.* **2008**, *47*, 6382–6392.
(33) Kapre, R.; Bothe, E.; Weyhermüller, T.; George, S. D.; Wieghardt, K. *Inorg. Chem.* **2007**, *46*, 5642–5650.
(34) Hwang, J.; Kim, E.-G.; Liu, J.; Brédas, J.-L.; Duggal, A.; Kahn, A. *J. Phys. Chem. C* **2006**, *111*, 1378–1384.
(35) Tengstedt, C.; Osikowicz, W.; Salaneck, W. R.; Parker, I. D.; Hsu, C.-H.; Fahlman, M. *Appl. Phys. Lett.* **2006**, *88*, 053502.
(36) Hwang, J.; Wan, A.; Kahn, A. *Mater. Sci. Eng., R.: Rep.* **2009**, *64*, 1–31.

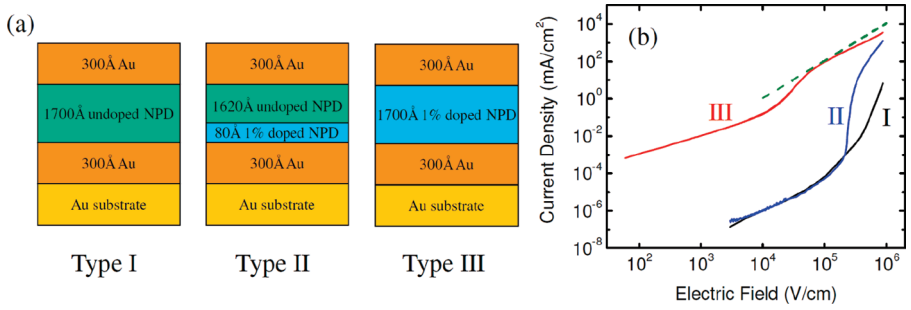

Figure 3. (a) Structure of the three device types. (b) $J-F$ characteristics of the three Au/α-NPD/Au devices. The bias polarity corresponds to holes injected from the bottom contact. The green dashed curve represents the SCLC limit calculated using a hole mobility of 6.1×10^{-4} cm^2/(V s) (see text).

which extends in the gap away from the edge of the HOMO (LUMO). (The acronym LUMO represents the lowest unoccupied molecular orbital.) These states, which also are present in the α-NPD film, become charged when the Fermi level approaches the HOMO (LUMO) edge.

The effect of doping on the α-NPD conductivity was investigated using $I-V$ measurements performed in situ on three types of hole-only devices made under UHV conditions. The structures are displayed in Figure 3a. All devices include freshly evaporated top and bottom Au contacts. The Type I device consists of a 1700-Å-thick undoped α-NPD layer. The Type II device is composed of a 80-Å-thick α-NPD layer doped with 1 mol % $Mo(tfd)_3$ and a 1620-Å-thick undoped α-NPD layer. Type III device is made of a 1700-Å-thick α-NPD layer homogeneously doped with 1 mol % $Mo(tfd)_3$.

The current density versus electric field ($J-F$) characteristics of the three devices are shown in Figure 3b. The bias polarity corresponds to holes injected from the bottom contact. The electron injection barrier at the top contact is extremely large (> 3 eV, given the nearly 4 eV gap of α-NPD[37,38]), ensuring a hole-only current. As expected, the Type I device shows the lowest current density. At low electric field ($F < 5 \times 10^4$ V/cm), the contribution of injected charge carriers is negligible, and the current regime is ohmic, as confirmed by the unit slope of the linear part of the $J-F$ curve on a log−log scale. Injection becomes more important at $> 5 \times 10^4$ V/cm. In that regime, the current in the Type I device can be modeled with the Richardson−Schottky thermionic emission equation:[2,39]

$$J = A^* T^2 \exp\left(-\frac{\phi_B - \beta\sqrt{F}}{\kappa_B T}\right) \quad (1)$$

where A^* is the Richardson constant ($A^* = 4\pi q m^* \kappa_B^2/h^3$), T is the temperature, $\beta = [q^3/(4\pi\varepsilon\varepsilon_0)]^{1/2}$, ϕ_B is the zero-field injection barrier, q is the elementary charge, m^* is the effective hole mass, κ_B is the Boltzmann constant, h is Planck's constant, ε_0 is the permittivity of free space, and ε is the relative dielectric constant of α-NPD ($\varepsilon \approx 3$).[40] The reduced experimental data, plotted in Figure 4 as $\log(J)$ versus $F^{0.5}$ for $F > 5 \times 10^4$ V/cm, follow a linear relationship over 6 orders of magnitude, in good agreement with expectations from eq 1. The injection barrier $\phi_B = 1.00$ eV, derived from the Y-axis intercept of the linear fit in Figure 4, is in accord with the UPS-determined injection barrier ($E_F - E_{HOMO}$) = 0.86 eV measured on the first 50 Å of the α-NPD film evaporated on a bottom Au contact (data not shown here). Note that the slight difference between this barrier and the 0.99 eV barrier previously mentioned results from common fluctuations in interface preparations.

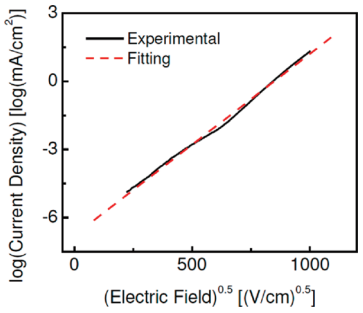

Figure 4. Fitting of the $J-F$ curve of the Type I device to the Richardson−Schottky thermionic emission equation plotted as current density versus (electric field)$^{0.5}$ on a log−linear scale.

In the Type II device, the impact of the narrow 80-Å-thick doped interface layer on the conductivity of the bulk of the 1700 Å film is expected to be minimal. This is indeed confirmed by the almost-perfect overlap of the $J-F$ characteristics of the Type II and Type I devices at low field ($F < 2\times10^5$ V/cm) (see Figure 3b). However, between 2×10^5 and 4×10^5 V/cm, the current density increases rapidly and reaches a value $\sim 2 \times 10^3$ times larger than that in the Type I device at a field of 3.5×10^5 V/cm. This is attributed to a significant reduction in the effective injection barrier, which is due to doping-induced formation of a narrow depletion region at the interface. This narrowing leads to significant carrier tunneling across the depletion region, which is far more efficient than thermionic emission over the barrier. This phenomenon, which has been observed previously in α-NPD[2] and copper phthalocyanine[41] doped with F_4-TCNQ, is one

(37) Hill, I. G.; Kahn, A.; Cornil, J.; Santos, D. A. D.; Brédas, J.-L. *Chem. Phys. Lett.* **2000**, *317*, 444–450.
(38) Hill, I. G.; Kahn, A.; Soos, Z. G.; Pascal, J. R. A. *Chem. Phys. Lett.* **2000**, *327*, 181–188.
(39) Murphy, E. L.; Good, R. H. *Phys. Rev.* **1956**, *102*, 1464–1473.
(40) Hermann, S.; Gordan, O. D.; Friedrich, M.; Zahn, D. R. T. *Phys. Status Solidi C* **2005**, *2*, 4037–4042.
(41) Gao, W.; Kahn, A. *Org. Electron.* **2002**, *3*, 53–63.

of the key advantages introduced by spatially confined interfacial doping. Interestingly, the field at which the current increases rapidly in the present study is very close to that found in a similar device fabricated using F_4-TCNQ as the *p*-dopant (4 V/1700 Å $= 2.4 \times 10^5$ V/cm).[2] To better understand the doping induced narrowing of depletion region, the depletion width is estimated as follows for the 1-mol %-doped α-NPD film. The total band bending in the 1-mol %-doped α-NPD film approximately equals the observed Fermi level difference between the undoped and 1-mol %-doped α-NPD films, i.e., 0.51 eV (recall Figure 2). This is similar to the value observed experimentally for F_4-TCNQ doped α-NPD (0.35 eV).[2] Assuming that the doping efficiecy is 100%, the depletion width at zero field can be estimated to be ~40 Å, based on the standard electrostatic model, $W = (2\varepsilon\varepsilon_0 V_{BB} M/qc\rho N_A)^{1/2}$ where V_{BB} is the total band bending ($V_{BB} = 0.51$ V), M is the molecular weight of α-NPD (in this case, $M = 589$ g), c is the doping concentation (here, $c = 1\%$), ρ is the density of α-NPD (here, $\rho = 1.2$ g/cm^3), and N_A is Avogadro's constant. Here, the estimated depletion width is comparable to that found experimentally in F_4-TCNQ-doped zinc phthalocyanine.[41] The increase in current density slows down at even higher fields, as transport approaches the space-charge limited current (SCLC) regime.

The current density in the Type III device is the highest among the three devices. Conductivity enhancement is observed over the entire electric field range and can be attributed primarily to the increase in hole density (α-NPD radical cations) afforded by doping and/or the filling of low mobility trap states by these holes. It is particularly prominent at low electric field, where ohmic conduction dominates. At $F = 10^4$ V/cm, the current densities in the Type I, Type II, and Type III devices are 1.0×10^{-6}, 9.4×10^{-7}, and 1.5×10^{-1} mA/cm^2, respectively (i.e., the enhancement is more than five orders of magnitude). This difference is reduced at higher field, as contributions from injected charge carriers and limitations due to space-charge effects in the SCLC regime take over.[2] The green dashed curve in Figure 3b represents the space-charge limited current density (SCLC) estimated according to the Mott−Gurney law,[42] i.e., $J = \frac{9\varepsilon\varepsilon_0\mu F^2}{8d}$, where d is the α-NPD film thickness (here, $d = 1700$ Å), F is the electric field, and μ is the mobility (here, $\mu = 6.1 \times 10^{-4}$ cm^2/(V s)).[43]

Figure 5 shows the $J-F$ characteristics of the three devices with bias polarity corresponding to hole injection from the top contact. The $J-F$ curve corresponding to hole injection from the bottom contact in the Type III device is also plotted as a reference. In both the Type I and Type II devices, the top contact is the vacuum-evaporated gold electrode interfacing with undoped α-NPD. Charge-carrier injection and transport are expected to be similar

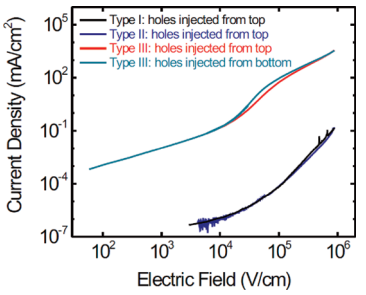

Figure 5. $J-F$ characteristics of the three Au/α-NPD/Au devices with bias polarity corresponding to hole injection from the top contact; the $J-F$ curve corresponding to bottom hole injection in the Type III device is also plotted as a reference.

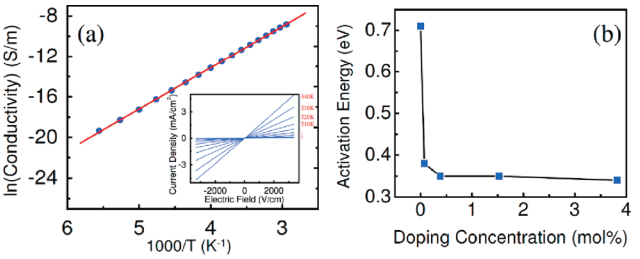

Figure 6. (a) Conductivity as a function of $1000/T$ for the 200-nm-thick α-NPD film doped with 1.7 mol % $Mo(tfd)_3$; the red line is a linear fit to the experimental data, and a representative set of $J-F$ curves acquired at different temperatures are plotted in the inset. (b) Activation energy extracted from the VTIV data as a function of the doping concentration; the black line serves as a guide to eyes.

in the two devices, as confirmed by the overlap of the two $J-F$ curves. The high field deviation due to enhanced injection observed in the bottom-injected Type II device (see Figure 3b) is absent, because neither of these two interfaces is doped and can support the tunneling previously mentioned. In the Type III device, however, both top and bottom gold electrodes are in contact with α-NPD:1 mol % $Mo(tfd)_3$, and the current density is orders of magnitude higher than that in the other two devices. Note that the top injection and bottom injection are identical on this device, compatible with the facts that (i) the two contacts interface with a doped semiconductor and, therefore, are less dependent on the interface barrier, and (ii) the organic-on-metal and the metal-on-organic interfaces are made under UHV conditions, which generally leads to identical barriers.[36,44]

To explore the low-field charge transport in doped α-NPD, VTIV measurements were performed on 200−500-nm-thick films doped with concentrations of $Mo(tfd)_3$ varying from 0 mol % to 3.8 mol %. A representative set of $J-F$ curves recorded at different temperatures are plotted in the inset of Figure 6a for a 200-nm-thick α-NPD:1.7 mol % $Mo(tfd)_3$ film. Data were collected down to 180 K for this sample, below which the measured current is dominated by noise. Between 180 K and 340 K, the $J-F$ curves are linear over the entire field range. The conductivity (σ) at different temperatures is extracted from the linear fit to the $J-F$ curves, and $\ln(\sigma)$ is plotted

(42) Pope M.; Swemberg, C. E. *Electronic Processes in Organic Crystal and Polymer*; Oxford University Press: Oxford, U.K., 1998.
(43) Brütting, W.; Riel, H.; Beierlein, T.; Riess, W. *J. Appl. Phys.* **2001**, *89*, 1704–1712.
(44) Wan, A.; Hwang, J.; Amy, F.; Kahn, A. *Org. Electron.* **2005**, *6*, 47–54.

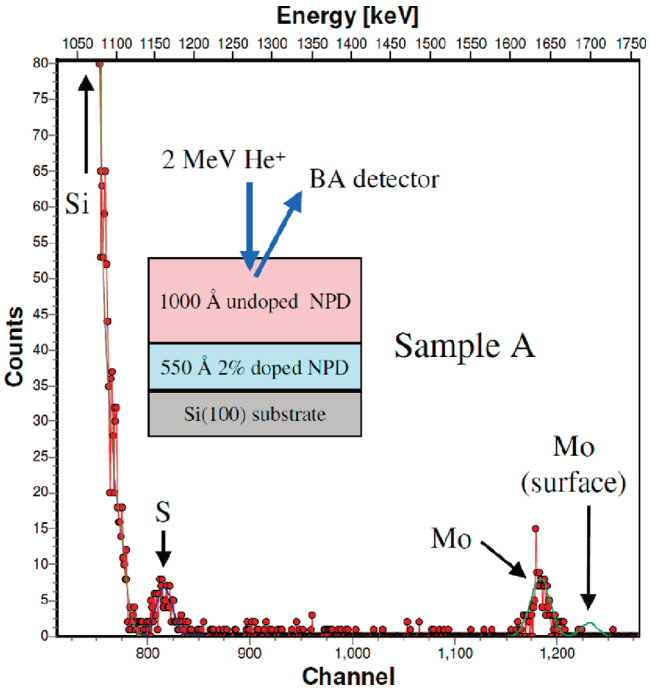

Figure 7. Expanded part of experimental RBS spectrum showing the Si, S, and Mo features and corresponding simulation (see text) for sample A (see structure in inset). The spectrum is taken with a typical BA detector.

as a function of $1000/T$ in Figure 6a. The maximum field used in these data is still in the ohmic regime, as discussed for Figure 3b; thus, the current is expected to be largely dominated by carriers induced by doping. According to various models of carrier hopping transport in amorphous molecular solids, such as variable range hopping,[45] the conductivity has a simple Arrhenius dependence on temperature, $\sigma = \sigma_0 \exp(-\frac{E_a}{k_B T})$ where σ_0 is a constant prefactor and E_a is the activation energy. The linear relationship between $\ln(\sigma)$ and $1000/T$ (see Figure 6a) is consistent with this model. Figure 6b shows the values of activation energy extracted from the VTIV data as a function of the doping concentration. The activation energy decreases from approximately 0.7 eV (undoped) to 0.35 eV (doping concentration = 0.4 mol %), and remains essentially constant for larger doping concentrations. The significant reduction in activation energy is consistent with preferential filling of the deep traps by holes introduced by dopants. Additional carriers in the system occupy shallower states, and less energy is required for activating hopping to neighboring sites.

The stability of the dopant in the organic matrix is a very important property for device application. Room-temperature diffusion of $Mo(tfd)_3$ in α-NPD was investigated via RBS measurements on sample A, which consists of a 55-nm-thick doped layer capped with a 100-nm-thick undoped layer (see inset in Figure 7). The energy (channel) region corresponding to He scattering from Si, S, and Mo from sample A is shown in the figure. The green curve is the simulation corresponding to the Mo peak, assuming no diffusion. The good agreement

(45) Vissenberg, M. C. J. M.; Matters, M. *Phys. Rev. B* **1998**, *57*, 12964–12967.

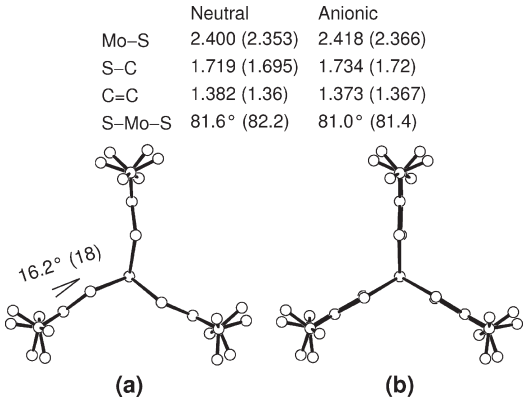

Figure 8. DFT-optimized geometries of (a) neutral and (b) anionic $Mo(tfd)_3$ viewed along the approximate molecular 3-fold axes. Numbers shown in parentheses are from X-ray crystallographic data (see refs 42 and 43). Bond lengths are given in Ångstroms.

between experimental data and simulation confirms the stability of Mo against diffusion at room temperature. The small simulated peak at channel 1230 is added to represent any Mo species that might have diffused to the surface of the organic film; it is important to note that no signal is detected at this energy. After correcting for the scattering cross section, the measured ratio between S and Mo is 6.25, which is very similar to that expected from the stoichiometry of $Mo(tfd)_3$, suggesting that the integrity of the dopant molecules (presumably the corresponding radical anions) is maintained in the host film.

To further examine the stability of $Mo(tfd)_3$ at elevated temperatures, RBS measurements were performed on samples annealed for 15 min in dry nitrogen at 70, 90, or 110 °C. The measured molecular concentration of $Mo(tfd)_3$ was 1.8 mol %, which is similar to the intended 2 mol % concentration. There was no detectable diffusion in any of the annealed samples. We estimate that a peak broadening of ~100 nm could be detected, thus setting a limit on the diffusivity of the $Mo(tfd)_3$. The excellent stability of the dopant toward diffusion, even at elevated temperatures, is presumably due to the bulkier and three-dimensional structure of $Mo(tfd)_3$, and this is a very positive point for device application.

To gain more insight into diffusional stability of $Mo(tfd)_3$ in α-NPD, as well as the energy levels of $Mo(tfd)_3$, DFT calculations were performed to obtain the geometries and electronic structures of isolated neutral and anionic $Mo(tfd)_3$ molecules. The DFT results reproduce well the experimental geometries of both neutral[46] and anionic[47] $Mo(tfd)_3$ previously obtained from X-ray crystallography (see Figure 8). Notably, each ligand in the neutral molecule is bent away from the S−Mo−S plane (at a "chelate fold" angle of 16.2°), making the dopant molecule relatively compact. These chelate folds disappear as the dopant accepts an electron. This "unfolding" of the molecule, along with an increase in Mo−S bond length by 0.02 Å, increases the molecular volume by more

(46) Wang, K.; McConnachie, J. M.; Stiefel, E. I. *Inorg. Chem.* **1999**, *38*, 4334–4341.
(47) Heuer, W. B.; Mountford, P.; Green, M. L. H.; Bott, S. G.; O'Hare, D.; Miller, J. S. *Chem. Mater.* **1990**, *2*, 764–772.

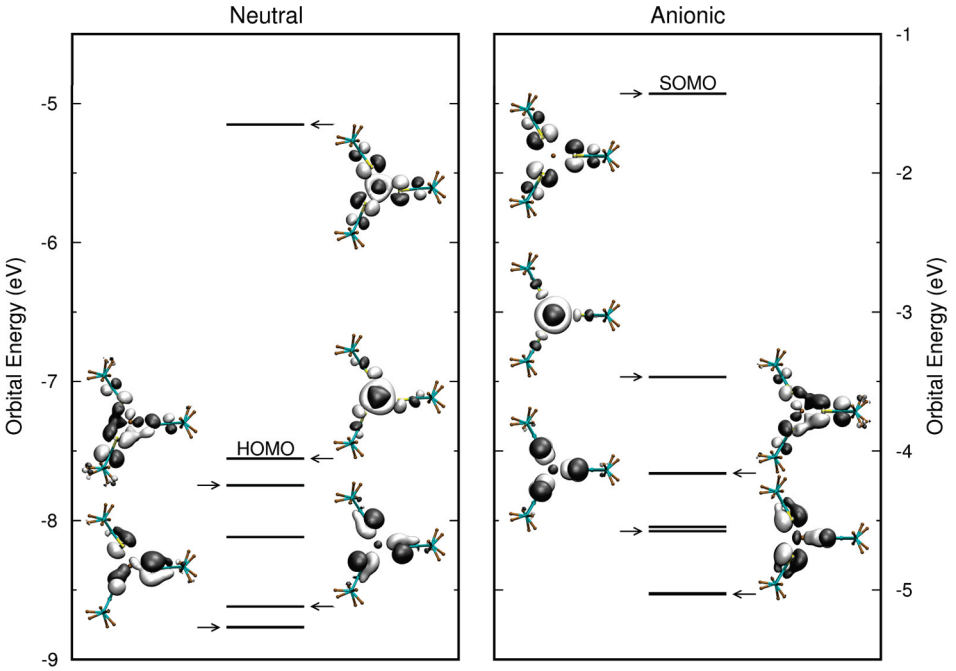

Figure 9. DFT-calculated frontier molecular orbital energy levels of neutral and anionic $Mo(tfd)_3$. Both the first and fourth levels from the bottom are almost doubly degenerate.

than 10%. The bulkier anion can be a favorable attribute for a dopant, with respect to anchoring of the dopant molecules within the host matrix upon doping; this is consistent with the stability of $Mo(tfd)_3$ against diffusion observed via RBS.

The frontier molecular orbitals of neutral $Mo(tfd)_3$ are shown in Figure 9, where the occupied levels contribute to the first two bands in the UPS spectrum.[20] Generally, the electron density is delocalized over both the metal and ligands; in the HOMO, the electron density is more localized on Mo (mostly of $4d_{z^2}$ nature) than on the dithiolene ligands, whereas it is the opposite for the lower energy levels. All Mo 4d atomic orbitals (d_{xy}, d_{xz}, d_{yz}, $d_{x^2-y^2}$, and d_{z^2}) are present in this energy range and, except for d_{z^2}, can also be found in deeper energy levels.

In the anion, the same occupied molecular orbitals are traceable, only with more symmetric spatial distribution on the ligands, partially due to the trigonal prismatic structure of the anion, which also affects the spacings between energy levels. The higher symmetry of the anion also precludes d_{z^2} contributions to the singly occupied molecular orbital (SOMO) and so the extra electron is accommodated on the ligands only. A similar picture in which the mixing of metal d_{z^2} and ligand orbitals is induced by the chelate fold has previously been described based on DFT calculations for the $Mo(mdt)_3$ (mdt = 1,2-dimethyl-1,2-dithiolene) system[32] and on the basis of Fenske−Hall calculations for unsubstituted molybdenum tris(1,2-dithiolene), although the ordering of the d_{z^2} and ligand orbitals in the absence of folding was reversed in the second study, relative to that found in $Mo(tfd)_3^-$ and $Mo(mdt)_3^-$.[48] These reduction characteristics of $Mo(tfd)_3$ highlight that the valence electronic configuration of Mo is influenced slightly by reduction ($5s^{0.3}4d^{5.9}5p^{1.0}$ for the neutral and $5s^{0.3}4d^{6.0}5p^{1.0}$ for the anionic species, from the natural population analysis). The d_{z^2} occupation increases slightly from 1.62 to 1.88. We note that the calculated oxidation state, obtained from the natural population analysis, should not be confused with the *formal* oxidation state, for which complete ionic bonding is assumed.[49] A large population of the 4d orbitals is an indication of significant covalent bonding between Mo and the ligands. The fact that the 4d occupation is similar in both neutral and anionic $Mo(tfd)_3$ is also consistent with the sulfur K-edge X-ray absorption spectroscopy analysis of $Mo(mdt)_3$ (mdt = 1,2-dimethyl-1,2-dithiolene) and its anion. [32]

4. Summary

In summary, we have shown that $Mo(tfd)_3$ can efficiently *p*-dope hole transport materials with highest occupied molecular orbital (HOMO) levels as deep as that of α-NPD and presumably up to 5.7−5.8 eV. Evidence of *p*-doping on α-NPD includes a significant shift of the Fermi level toward the α-NPD HOMO level and enhanced hole injection and conductivity. Variable-temperature current−voltage measurements reveal that the low-field conductivity of the $Mo(tfd)_3$-doped α-NPD films can be described by a thermally activated polaron hopping model, with an activation energy that logically decreases with doping, as deep traps are being filled. The very good stability of $Mo(tfd)_3$ molecules against diffusion in α-NPD, even at elevated temperature, confirmed by Rutherford backscattering (RBS), makes this

(48) Campbell, S.; Harris, S. *Inorg. Chem.* **1996**, *32*, 3285–3288.

(49) Kaupp, M.; von Schnering, H. G. *Angew. Chem., Int. Ed.* **1995**, *34*, 986.

dopant a suitable choice for device applications. Density functional theory (DFT) calculations reveal a size increase of $Mo(tfd)_3$ upon doping, which further supports the diffusional stability of the dopant.

Acknowledgment. Support of this work by Solvay, the National Science Foundation (DMR-0705920), and the Department of Energy (DE-FG02-04ER46165) is gratefully acknowledged.